Transition Metal Adatoms on Graphene: A Systematic Density Functional Study

Montserrat Manadé, Francesc Viñes,* and Francesc Illas

Departament de Química Física & Institut de Química Teòrica i Computacional (IQTCUB), Universitat de Barcelona, c/Martí i Franquès 1,08028 Barcelona, Spain.

Abstract

Transition Metal (*TM*) atom adsorption on graphene results in a tuning of their electronic, magnetic, storage, sensing, and catalytic properties. Herein we provide a thorough density functional theory study, including dispersion, of the structural, energetic, diffusivity, magnetic, and doping properties for *all* 3*d*, 4*d*, and 5*d* TM adatoms adsorbed on graphene. TMs prefer to sit on hollow sites when chemisorbed, but on bridge or top sites when physisorbed; which is the case of atoms with d^5 and d^{10} configurations. Diffusion energy barriers follow the adsorption energy trends. Dispersive forces simply increase the adsorption strength by ~0.35 eV. Adatom height seems to be governed by the bond strength. All TMs are found to *n*-dope graphene, except Au, which *p*-dopes. The electron transfer decays along the *d* series due to the electronegativity increase. Early TMs infer noticeable magnetism to graphene, yet for elements with more than five electrons in the *d* shell the local magnetic moments abruptly decay to low or zero values. Experimental observations on adatom position, height, temperature clustering and Ostwald ripening, *p*- or *n*-doping, or the electronic configuration can be rationalized by present calculations, which deliver a solid theoretical ground from which experimental features can be interpreted and discussed.

*Corresponding Author: Tel: +34 93 403 37 07, e-mail: francesc.vines@ub.edu

1. Introduction

In the last decade graphene —a single layer of graphite— has become a material of exceptional interest in many research areas, mainly due to its unique electronic bandstructure, featuring Dirac cones where charge carriers feature ballistic transport properties [1,2], but also due to its exceptional physical properties, including high chemical and thermal stabilities, and mechanical strength [3]. All this poses graphene as the material of the foreseeable future in nanotechnology. The attachment of small moieties on graphene, such as molecules or small metal clusters, has attracted many research endeavours owing, for instance, to the synthesis of graphene derivatives like graphene oxide, graphane, and fluorographene [4-6], the graphene bandstructure engineering [7,8], its utilization as a nanosensing material [9], and, also, to its use as a support for highly and uniformly dispersed metal aggregates relevant for catalysis [10-13].

Lately, transition metal atoms deposited on carbon surfaces have attracted considerable interest in the fields of molecular sensing [14-16], hydrogen storage [17-19], transistors [20], catalysis [21-23], metal nanowire synthesis [24], and nanoelectronics [25]. Aside from this, graphene is by itself a promising material for spintronics given the controllable spin transport [26], its perfect spin filtering [27], and the spin-relaxation lengths in the order of the micrometre at standard conditions [28], due to the very weak spin-orbit coupling in carbon [29]. In this sense the adsorption of transition metal atoms on graphene is a field of interest due to the possibility of bestowing magnetism [30], differentiating the transport properties of the spin channels [31], or ionizing the adatom by the plugging of a gate voltage [32], with remarkable implications for the usage of such systems in spintronics [33,34], nanomagnets [35], and data storage [30].

On this basis, studies on the adsorption of transition metal atoms on graphene have grown importance in the last years both from the experimental and theoretical point of views.

Experimental reports are somewhat scarce mainly due to technical difficulties; nonetheless, transition metal adatoms tend to diffuse and aggregate at room temperature, forming clusters and nanoparticles, a matter which is itself the focus of experimental research [36,37] and also first-principles simulations [38]. Anyway, in order to effectively have isolated adatoms temperatures in the 4-20 K range are required to avoid adatom diffusion and aggregation. Under these conditions it is worth to mention the work of Gierz *et al.* [39], who by means of Angle-Resolved Ultraviolet Photoemission Spectroscopy (*ARUPS*) observed the graphene *n*- or *p*-doping when depositing Bi, Sb, or Au atoms. Also remarkable is the research of Brar and coworkers [32] showing that the electronic structure of Co adatoms supported on graphene could be tuned by applying a gate voltage. A related study by Chen *et al.* [40] explains the minimum conductivity of graphene in terms of charged impurities, in that case, K adatoms.

Very important are also the works of Eelbo *et al.* [41] and Gyamfi *et al.* [42], who were able to deposit Ni and Co atoms on SiC(0001) pristine surface epitaxial Monolayer Graphene (*MLG*) and Quasi Freestanding MLG (*QFMLG*), and observed the corresponding atomic structure by means of Scanning Tunneling Microscopy (*STM*), using in addition local resonances as fingerprints to assign the adsorption sites [43]. The usage of this technique in combination with X-Ray Magnetic Circular Dichroism (*XMCD*) permitted Eelbo and coworkers not only to obtain structural information of Fe, Co, and Ni adatoms, but also insights on their magnetic properties [44].

Extensive works have been also carried out from the theoretical point of view addressing the interaction of one or more types of TM atoms on graphene, most within Density Functional (*DF*) theory. Fig. 1 shows, itemized, the number of published works for each given TM (for a detailed referencing and searching procedure we address the reader to Table S1 in the Supplementary Material). Note that 3*d* TMs have driven much more consideration compared to 4*d* and 5*d* ones. Indeed, the possibility of varying at will the

oxidation state of Co adatoms [32], or the coexistence of different adsorption configurations [44] have generated a great debate and numerous works solely for Co [45-47]. For 4*d* and 5*d* metals, the studies restrict mainly to Pt-group and coinage metals, such as Ag and Au, typically used in catalysis.

Figure 1: Sketch showing, colour-coded, the number of publications that studied for each 3*d*, 4*d*, or 5*d* TM its adsorption on graphene by means of periodic DF calculations.

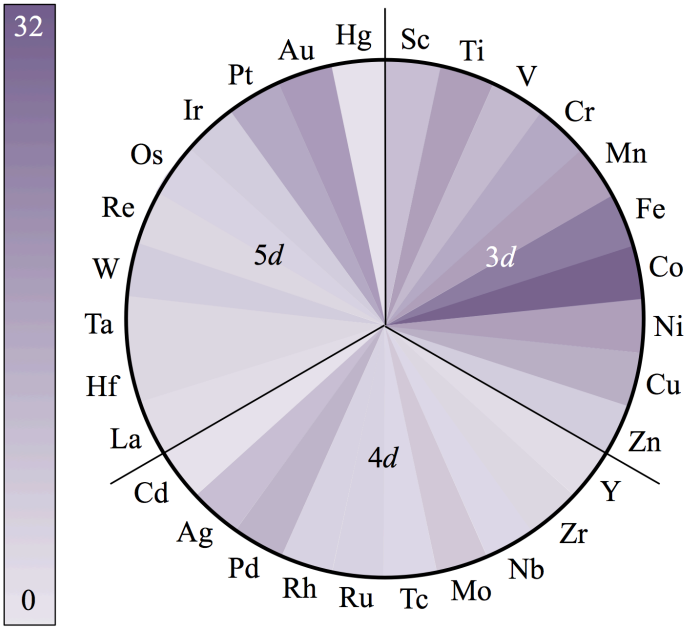

Most of the research, as above-commented, mainly addresses the adsorption of 3*d* TMs on graphene in terms of structural, energetic, electronic, and magnetic properties [48-50], typically obtained using an exchange-correlation (*xc*) DF within the Generalized Gradient Approximation (*GGA*). Other works have extended the study to acquire estimates of adatom diffusion energy barriers [51-53]. Some studies, yet relevant, implied some gross approximations. For instance, Wang *et al.* [54] studied the 3*d* transition metals adsorption on graphene using a xc within Local Density Approximation (*LDA*), presumably to counteract

the deficiency of GGA xc functionals in treating dispersive forces interactions. This strategy was also adopted by Ding *et al.* [55] to simulate the adsorption of late TMs on graphene, since in these cases the van der Waals (*vdW*) contribution is thought to be primordial. However, Ishii *et al.* [56] combined results from LDA or GGA approximations with no apparent justification, fact that is questionable though.

On the other hand, compared to 3*d* TMs, the 4*d* and 5*d* ones have been much less studied. Zhang *et al.* [57] did a precise study of the magnetic properties of many 5*d* metals at different coverages —ranging 0.03 to 0.13 monolayers (ML) and considering a full ML when a 1:1 TM:C ratio is achieved— but by deliberately placing the adatoms at hollow positions. Zólyomi *et al.* [58] studied the energetics, structure, and magnetic properties for 4*d* and 5*d* metals, but at a high coverage of 0.17 ML, *i.e.* having non-negligible interaction among TM adatoms. Finally, Habenicht *et al.* [59] studied structural, energetic, and diffusivity properties of 4*d* and 5*d* TM adatoms on graphene at a relatively low coverage of 0.06 ML, yet neglecting the spin polarization, *i.e.* considering the TM adatoms diamagnetic, which represents quite an oversimplification.

Note that, to the best of our knowledge, there is a single previous work consistently dealing with the adsorption structural, energetic, and diffusivity properties of *all* 3*d*, 4*d*, and 5*d* TMs on graphene [60]. This constitutes a reference study but one must advert that the whole study was carried out using certain approximations that are debatable. First, it was carried out for a 0.06 ML coverage, where adatoms can feature long-range magnetic coupling or even coulombic interactions whenever charged. However the magnetic coupling was disregarded since spin polarization was neglected. Finally, the calculations were carried out systematically at LDA level, which, as commented above, grossly serves to mimic the effect of vdW interactions although for the wrong physical reason. In fact, only few studies dealt with an explicit treatment of vdW interactions, and only for few TM adatoms [45,61-63].

The intent of this study is to provide a comprehensive study on the structural, energetic, diffusivity, magnetic, and electronic properties for the *full* sets of 3*d*, 4*d*, and 5*d* TM adatoms adsorbed on graphene. This has been carried out at a standard DF GGA level, but also including a proper vdW description, in order to get insights of whether dispersive forces interactions play a key role on these systems. The behavioural trends gained from these calculations provide a theoretical background solid as a rock from which observed experimental features can be interpreted, understood, and discussed.

2. Computational Details

Spin polarized DF calculations have been performed using the Vienna *Ab initio* Simulation Package —VASP [64]. The Projector Augmented Wave (*PAW*) method has been used to represent atomic cores effect on the valence electron density [65]. This simulation of the core states allows one to obtain converged results —energy variations below 0.01 kJ mol^{-1}— with a cut-off kinetic energy of 415 eV for the plane-wave basis set. Geometry optimizations were performed using a conjugated gradient algorithm and applying a first-order Methfessel-Paxton smearing of 0.2 eV width, yet final energies were corrected to 0 K (no smearing). The structural optimizations were finalized when forces acting on atoms were below 0.01 eV $Å^{-1}$. All DF calculations have been carried out using the Perdew-Burke-Ernzerhof (*PBE*) xc functional [66], a representative of GGA ones. This functional has been previously found to essentially match the graphene cell parameter of 2.46 Å [67], and also to yield the best overall description of TMs among many LDA, GGA, meta-GGA, and hybrid functionals [68,69].

Energy and structure optimizations have been carried out on a $p(4\times4)$ slab supercell, since it grants a separation between adsorbed adatoms of ~1 nm, enough to avoid interactions with TM adatoms on periodically repeated adjacent cells. According to test calculations lateral interactions are estimated to be below 0.03 eV. For this supercell size the TM atomic

coverage is ~0.03 ML. A vacuum region of 1 nm is added in the direction normal to the graphene layer, in order to avoid interactions between repeated slabs. Test calculations with double vacuum yielded variations in the energy of ~0.003 eV. An optimal Monkhorst-Pack [70] **Γ**-centred **k**-point grid of 2×2×1 dimensions was used, having a similar **k**-point density as in earlier reports [67].

Mind that for any TM atom adsorbed on graphene the adsorption energy, E_{ads}, is defined as

$$E_{ads} = (E_G + E_{TM}) - E_{TM/G} \quad (1),$$

where $E_{TM/G}$ is the total energy of graphene layer with the TM adatom attached, E_G is the total energy of the pristine graphene layer, and E_{TM} the total energy of an isolated TM atom as previously calculated [68]. Thus, adsorption energies are defined positive, and hence, the larger the E_{ads} value, the stronger the interaction between graphene and the TM atom. Charges on TM adatoms, Q, which are necessarily related to the oxidation state, have been estimated through a Bader analysis of the electron density [71]. Adatom height, h, has been calculated with respect to the mean plane of the graphene sheet. The graphene corrugation, c, has been estimated by subtracting the height of the highest C atom from that of the lowest, and defining it positive whenever the graphene layer approaches to the TM adatom, *i.e.* forming a hill where TM adatom sits atop, and, *vice versa*, negative whenever graphene is repelled from the TM adatom, forming a valley which embraces the TM adatom.

Adatom diffusion is a vital process in its tethering to a surface and to the related cluster formation processes. Because of this diffusion, transition states have been obtained in a stepwise fashion: this is, paths connecting high symmetry adsorption sites have been sampled by obtaining the energy of a TM over this site. This is simple for minima and Transition States (*TS*), but points with an energy gradient have been obtained with a restricted optimization, where the adatom plane position is kept fixed, as well as that most distant C

atom is kept frozen, whereas all other degrees of freedom are allowed to relax. In this way, the fixed C atom serves as an anchor to the graphene sheet, avoiding its sliding to accommodate the TM adatom in a minimum. For most of the systems one highly symmetric site is already a TM diffusion TS. These minima and TSs have been characterized by a vibrational frequency analysis when needed, obtained by construction and diagonalization of the Hessian matrix by finite differences of analytical gradients with individual displacements of 3 pm in each cell direction, and including both TM and graphene sheet atoms. All found minima feature only positive eigenvalues, and TSs only an imaginary frequency. Note that in some cases a suspect TS has been obtained by sampling more points in its vicinity. Finally, in a few cases the TS character has been also identified with a forth and back displacement of the TM followed by a full relaxation, observing that these two systems evolve to the two nearby minima connected through the TS. Diffusion energies have been estimated by the simple difference in energy between the located TS and the most stable adsorption site.

Description of the vdW dispersive forces has been accounted for *via* the D2 dispersion correction of Grimme [72]. This particular vdW correction has been found to be one of the best choices for the interaction of graphene with TM surfaces [67], as well as previous calculations on few selected cases showed a nice agreement with other vdW-DF approximations [62,63]. Moreover, the PBE-D2 combination has been found to be a good tandem in the description of the attachment of graphene on a TM surface [67]. Note that here dispersion coefficients, C_6, and vdW radii, R_0, were collected from the original paper for 3*d* and 4*d* TMs [72], and those for 5*d* metals were taken from a posterior study [62].

3. Results and Discussion

At first, standard DF PBE calculations are put under light. The adsorption of TM atoms on graphene has been studied on several graphene sites, including the highly symmetric sites Top (T), Bridge (B), and Hollow (H), as depicted in Fig. 2a, but other lower symmetry

sites have been sampled, including that at half-distance from T to H (h_1), and those at $^1/_3$ and $^2/_3$ of the distance from B to H (h_2 and h_3, respectively), see Fig. 2a. However, these last low symmetry sites tend to evolve to any of the highly symmetric ones, and so have not been further discussed —with the caveat of h_1 for Ir adatom. The diffusion energy barriers have been sampled in a stepwise fashion as depicted in the computational details section following the tuck-turn path depicted in Fig. 2b. This triple step path scans B→T, T→H, and H→B diffusions. Fig. 3 illustrates the Sc case as an illustrative example of the adatom diffusion.

Figure 2: Schematic representation of a) the adsorption sites of an atom on graphene —labelled yellow spheres— and b) the explored diffusion path of an adatom on graphene —orange arrow. Dashed fine orange lines guide the eye on the hexagonal structure of graphene, and the triangles these hexagons contain.

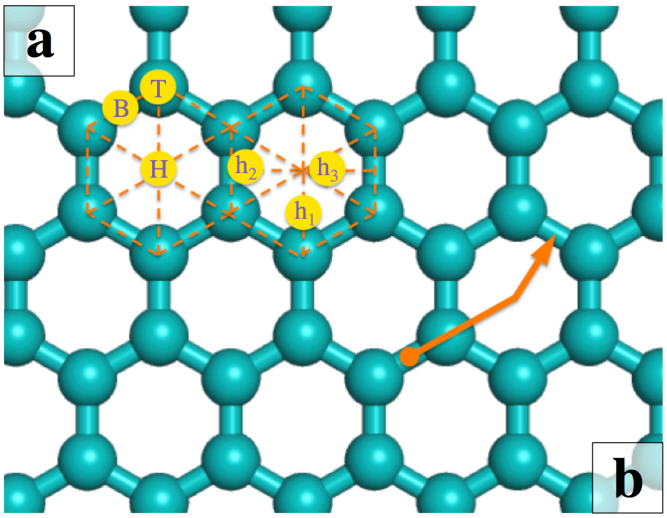

Figure 3: Sc adatom diffusion energy profile on graphene as obtained at PBE level. Labels denote high and low symmetry adsorption sites. Note that here, at variance with the discussion, negative values for E_{ads} are plotted, to better show the minima and TS characters of certain adsorption sites.

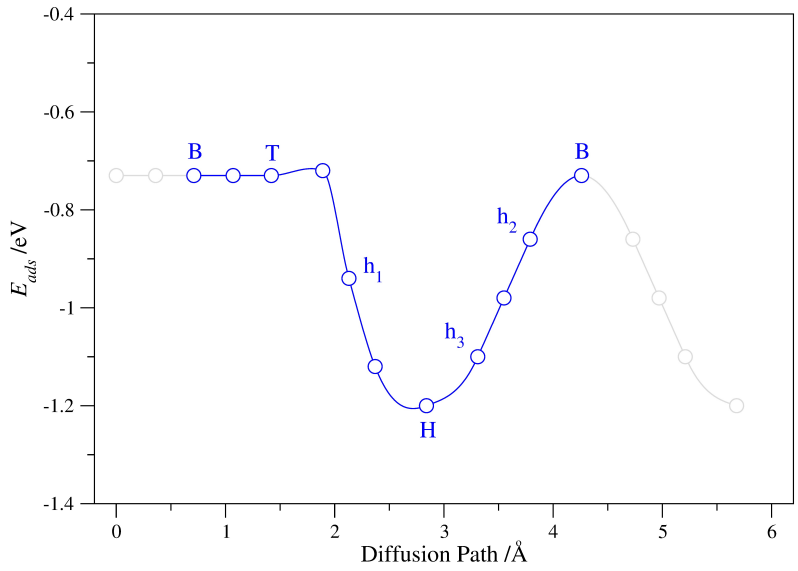

Noted this, Table 1 encompasses, for each TM adatom, the most stable site and its adsorption energy, together with its height from the graphene layer and the graphene sheet corrugation. For each TM, the lowest energy diffusion path serves to acquire the diffusion energy barrier estimate, E_{dif}. In addition, the TM charge, Q, triggered by a TM→graphene charge transfer, is listed —note that the electron accumulation (depletion) on (from) graphene involves in all cases a delocalized state for graphene. Finally, the variations on TM adatom magnetic moment due to the adsorption process, $\Delta\mu$, and the overall local magnetic moment, μ, are also encompassed on Table 1. Alongside, Table 2 gathers the same results as in Table 1 but obtained from PBE-D2 calculations.

3a. Energetic Properties

Energetic trends are now analysed, beginning by the adsorption strength, E_{ads}. From Fig. 4 it is apparent that the evolution along the *d* series follows a camel humps shape. This is

mostly due to a rather low adsorption energy, below 0.5 eV —characteristic of a physisorption situation—, for TMs of groups VI, VII, XI, and XII. Note that these elements are generally characterized by having a semi or full occupancy of *d* orbitals, *i.e.* they display a d^5 or d^{10} electronic configuration. These are known to stabilize the isolated atom, and, consequently, its binding strength to graphene is low. This hand-to-hand reasoning is also valid for the rest of the TMs, whose more unstable electronic configurations makes them attach stronger to the graphene sheet, with values ranging 0.75-2.25 eV, and thus, most of them could be classified as chemisorption situations.

Thus, the adsorption strength seems to be governed by the relative (in)stability of the isolated TM atoms, and most of the cases adjust to this rule-of-a-thumb. Note, for instance, that the relatively high adsorption energies for W and Tc of 0.41 and 0.99 eV, respectively, can be tracked down to their d^4 and d^6 electronic configurations, respectively [68]. The exception to this rule is Pd, whose d^{10} configuration should yield a small adsorption energy, but it is found to be 1.08 eV at PBE level. In any case the adsorption energy is smaller than other group X TMs, such as Ni and Pt, with d^8 and d^9 configurations.

Present calculations can be compared to previous ones carrying out a more systematic analysis. Let us begin with the work of Ishii *et al.* [56]. Their calculations at PBE level showed large adsorption energy values, which differ by 1.24 eV in mean absolute values with present ones, with a standard deviation σ = 1.74 eV. This is, the E_{ads} values are consistently larger than present PBE calculations, *a priori* because of the usage of simplified ultrasoft (*US*) pseudopotentials instead of PAW, or, more likely, because of the neglecting of the spin polarization, which would lead to an unphysical description of the isolated atoms resulting in a too high energy and a concomitant exceedingly large adsorption energy. The usage of a larger coverage of 0.06 ML would only be detrimental of the adsorption strength, due to lateral adatom interactions. In the posterior study by Nakada and Ishii [60] this procedure was

Table 1: Summary of PBE calculated results for 3*d*, 4*d*, and 5*d* TM on graphene including the most stable adsorption site, adsorption energy, E_{ads}, and diffusion energy, E_{dif}, TM height from graphene, *h*, and graphene corrugation, *c*, TM adatom net charge, Q, and total magnetic moment of the system, μ, as well as variation of the magnetic moment with respect to the isolated TM atom. Energies are in eV, distances in Å, Q in a.u., and μ and $\Delta\mu$ are given in μ_B.

TM	**Site**	E_{ads} **/eV**	h **/Å**	c **/Å**	Q **/e**	$\Delta\mu$ **/μ_B**	μ **/μ_B**	E_{dif}**/eV**
Sc	H	1.20	1.96	-0.03	0.99	0.99	1.99	0.47
Ti	H	1.90	1.81	-0.02	1.01	1.00	3.00	0.58
V	H	1.60	1.82	-0.02	0.14	1.20	4.20	0.23
Cr	B	0.17	2.34	0.07	0.43	-0.33	5.67	0.01
Mn	T	0.09	2.23	0.03	0.53	0.33	5.33	0.02
Fe	H	0.73	1.53	-0.02	0.43	-2.00	2.00	0.59
Co	H	1.11	1.50	-0.04	0.38	-2.02	0.98	0.47
Ni	H	1.68	1.54	-0.02	0.45	-2.00	0.00	0.22
Cu	T	0.23	2.26	0.16	0.22	-0.02	0.98	0.01
Zn	H	0.03	3.85	0.00	0.02	0.00	0.00	0.00
Y	H	1.36	2.12	-0.02	1.12	1.01	2.01	0.32
Zr	H	2.11	1.96	-0.02	1.34	1.01	3.01	0.62
Nb	H	1.20	1.94	-0.02	0.79	-0.96	4.04	0.27
Mo	B	0.08	2.42	0.10	0.46	-0.49	5.51	0.00
Tc	H	0.99	1.63	-0.06	0.95	-4.08	0.92	0.54
Ru	H	1.52	1.74	-0.01	0.51	-2.00	2.00	0.62
Rh	H	1.62	1.81	-0.02	0.45	-2.01	0.99	0.19
Pd	B	1.08	2.21	0.21	0.27	0.00	0.00	0.04
Ag	B	0.03	3.63	0.00	0.03	-0.03	0.97	0.00
Cd	T	0.04	4.27	0.00	0.02	0.00	0.00	0.00
La	H	1.64	2.22	-0.04	1.46	1.07	2.07	0.35
Hf	H	1.50	1.90	-0.03	1.46	1.04	3.04	0.43
Ta	H	1.70	1.85	-0.03	1.29	0.74	3.74	0.69
W	B	0.41	2.31	0.12	0.93	1.56	5.56	0.02
Re	B	0.04	4.09	0.01	0.04	0.01	5.01	0.00
Os	H	0.87	1.70	-0.02	0.31	-1.97	2.03	0.41
Ir	h_1	1.04	1.97	0.25	0.21	-2.96	0.04	0.02
Pt	B	1.49	2.23	0.34	0.13	-2.00	0.00	0.18
Au	T	0.11	2.66	0.16	-0.07	0.05	1.05	0.02
Hg	T	0.03	4.13	0.01	0.01	0.00	0.00	0.00

Table 2: Summary of PBE-D2 calculated results for 3*d*, 4*d*, and 5*d* TM on graphene including the most stable adsorption site. Reported properties and units are as in Table 1.

TM	Site	E_{ads} /eV	h /Å	c /Å	Q /e	$\Delta\mu$ /μ_B	μ /μ_B	E_{dif}/eV
Sc	H	1.46	1.93	-0.06	1.00	0.98	1.98	0.41
Ti	H	2.17	1.78	-0.06	1.20	0.99	2.99	0.51
V	H	1.88	1.78	-0.05	1.00	1.14	4.14	0.21
Cr	B	0.47	2.32	0.05	0.47	-0.35	5.65	0.01
Mn	T	0.40	2.19	0.01	0.43	0.33	5.33	0.02
Fe	H	1.04	1.51	-0.03	0.84	-2.00	2.00	0.58
Co	H	1.41	1.49	-0.05	0.65	-2.01	0.99	0.47
Ni	H	1.98	1.53	-0.03	0.55	-2.00	0.00	0.23
Cu	T	0.53	2.21	0.13	0.15	-0.03	0.97	0.01
Zn	H	0.21	3.11	-0.02	0.02	0.00	0.00	0.01
Y	H	1.71	2.09	-0.05	1.07	1.01	2.01	0.25
Zr	H	2.48	1.92	-0.06	1.39	1.02	3.02	0.54
Nb	H	1.68	1.69	-0.05	0.83	-4.97	1.03	0.34
Mo	B	0.48	2.40	0.07	0.47	-0.51	5.49	0.01
Tc	H	1.41	1.61	-0.08	0.96	-4.11	0.89	0.56
Ru	H	1.91	1.71	-0.02	0.64	-2.01	1.99	0.62
Rh	H	2.01	1.78	-0.01	0.45	-2.03	0.97	0.19
Pd	B	1.47	2.21	0.20	0.24	0.00	0.00	0.01
Ag	B	0.35	2.97	0.02	0.05	0.00	1.00	0.00
Cd	T	0.26	3.31	0.02	0.02	0.00	0.00	0.00
La	H	2.04	2.18	-0.08	1.12	1.07	2.07	0.30
Hf	H	1.94	1.89	-0.06	1.58	-0.03	1.97	0.41
Ta	H	2.15	1.77	-0.06	1.41	-1.99	1.01	0.68
W	B	0.84	2.30	0.10	0.56	1.57	5.57	0.02
Re	T	0.36	3.16	0.04	0.04	-0.01	4.99	0.11
Os	H	1.33	1.68	-0.03	0.62	-1.97	2.03	0.44
Ir	h_1	1.52	2.00	0.24	0.26	-1.99	1.01	0.06
Pt	B	1.91	2.22	0.34	0.09	-2.00	0.00	0.15
Au	T	0.54	2.57	0.14	0.00	0.04	1.04	0.02
Hg	H	0.34	3.22	-0.02	0.01	0.00	0.00	0.07

used by carrying out LDA calculations, which yielded even larger deviations of 2.07 ± 1.51 eV with respect to the present work. In this sense, compared to PBE+D2, the utilization of LDA xc functionals seems to overbind TMs on graphene by ~0.8 eV, in average.

Figure 4: Adsorption energy (E_{ads}) of 3*d*, 4*d*, and 5*d* TM atoms on graphene, as well diffusion energies, E_{dif}, both in eV. Shown are the PBE (open circles and solid lines) and PBE-D2 (filled circles and dashed lines) DF results.

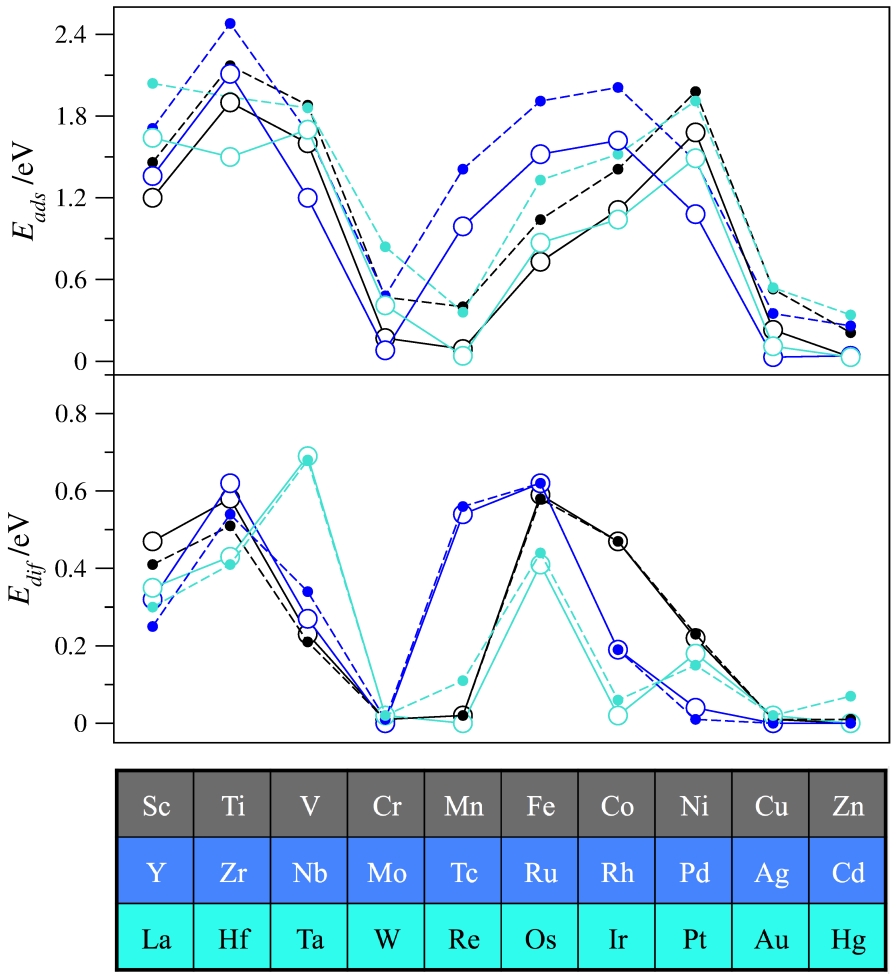

The study by Zólyomi *et al*. [58] was also carried at PBE level, but at a significantly higher coverage of 0.17 ML. In this case the previous E_{ads} values are also higher than the present ones by 0.43 ± 0.37 eV. Note that this would naively go against the lateral steric repulsion at a significantly higher coverage, although one can as well expect that the supported TM adatoms interact among themselves starting to form a metallic overlayer, as similarly found for other supported metal monolayers [73]. All electron scalar or full relativistic calculations at PBE level with a local orbital basis set, as those carried by Sargolzaei and Gudarzi [49], yields adsorption energies systematically smaller by 0.67 ± 0.32

eV. Better agreement is found when comparing to studies using the same basis set and pseudopotentials, although even in that situation some differences can be invoked. For instance, the main difference by Zhang *et al*. [50] is the finite model employed, which restricts the graphene bandstructure delocalization. This quantum confinement and the smaller coverage of 0.02 ML could be the origin of discrepancies of the order of 0.20 ± 0.22 eV.

This latter effect seem to be of the same order than using a different xc functional but still within GGA. This is the case of works by Valencia *et al*. [48] and Ding *et al*. [55], who employed the Perdew-Wang (PW91) xc functional in their calculations, which yielded variations of 0.20 ± 0.20 eV, at variance with bulk TM calculations, where variations in E_{coh} between PBE and PW91 were below 0.05 eV in average [68], here seems that the choice of one or another GGA functional is more accentuated, but still at the threshold of standard DF accuracy. The effect on the usage of simpler US pseudopotentials instead of PAW is perhaps more tangible inspecting the works by Hu *et al*. [52] and Yayzev *et al.* [51], with variations also of 0.20 ± 0.20 eV, although one has to keep in mind that in these last works slightly higher coverages of 0.04 and 0.06 ML were employed.

Indeed best agreement with present results is found for those combining PAW and PBE, as expected. It is worth to mention the study by Habenicht *et al*. [59] and Liu *et al*. [53], the former focused on 4*d* and 5*d* transition metals, whereas the latter is more focused on 3*d* TMs. The discrepancies with these works are minimal, of 0.10 ± 0.10 eV. The main discrepancies on 4*d* and 5*d* TMs are Nb and La, which, according to the previous work [59] feature E_{ads} values 0.39 and 0.33 eV larger, respectively, whereas the rest of TMs are within standard DF accuracy. Considering 3*d* TMs [53], the only disagreement is V, which according to present calculations binds to graphene 0.49 eV stronger.

Back to the camel humps shape obtained for E_{ads} values, the trend seems to be maintained for the diffusion energy barrier estimates. As observed in Fig. 4, E_{dif} is relatively

large whenever the adsorption strength is large, and *vice versa*. Thus, d^5 and d^{10} TMs feature almost insignificant diffusion energy barriers, below 0.02 eV, which would make think that such TMs are extremely mobile even at temperatures of few K. In this sense, *e.g.* a study by STM means of Au adatoms on graphene, as carried out for Fe, Co, and Ni [41,42,44], is problematic, given the Au high diffusivity; consequently, its study is restricted to spectroscopies, such as the ARUPS study of Gierz *et al*. [39].

The relationship of E_{ads} and E_{dif} has its outliers as well, and regretfully they prevent a useful linear relationship in between these two quantities. For instance, as above commented, d^4 W features a relatively higher E_{ads} compared to other group VI d^5 TMs Cr and Mo. However, the diffusion energy barrier is as low as 0.02 eV, more in accordance to a d^5 situation. In a similar way Ir and Pd atoms display high adsorption energies, but rather small E_{dif} values of 0.02 and 0.04 eV, respectively. Thus, an Ir or Pd atom would skip up over the graphene surface even at ultra-low temperatures. Other TMs, on the other hand, feature relatively high diffusion energy barriers yet attachment strengths are moderate. This is the case of Ta, which has an E_{dif} of ~0.7 eV, sensibly higher than the other group V TMs V and Nb, that have values of ~0.25 eV. Another example is Tc, which has a diffusion energy barrier of ~0.55 eV, given that is a d^6 element, at variance to the d^5 configuration of the other two group VI TMs, Mn and Re. Ta and Tc adatoms are thought to be rather immobile at cryogenic or even higher temperatures.

Present DF PBE estimates of the E_{dif} are, in overall terms, in excellent agreement with previous estimates. Here one must exclude however the PBE and LDA studies of Ishii [56] and Nakada [60], since deliver higher diffusion energy barriers by 0.26 ± 0.46 and 0.39 ± 0.47 eV, respectively. The discrepancy can be argued on the same terms as E_{ads} values were previously discussed. However, the difference is much more attenuated for other GGA works, reaching a perfect match with the PW91 estimates from Valencia *et al.* [48], with a deviation

of solely 0.01 ± 0.01 eV. For other works at PBE level the mean deviations are of 0.05 ± 0.05 eV [52,53,59], highlighting the excellent agreement. Actually, one could only raise few discrepancies, such as that present estimate of E_{dif} for Nb is 0.28 eV higher than a previous report [59], or that another work where Fe diffusion was found to be easier by 0.24 eV, but Mo diffusion more difficult by 0.22 eV [52].

The comparison between the TM adsorption energy and the bulk cohesive energy, E_{coh}, which can be taken from the literature obtained using an equivalent computational level of theory [68], determines whether TM adatoms are thermodynamically driven to coalesce and form metal clusters, given that metal↔metal bond strength is larger than metal↔carbon bond one, or the opposite whenever metal↔carbon bonds prevail. For any of the studied cases, the formation of clusters, aggregates, or even larger nanoparticles is, with no doubt, thermodynamically preferred. However, this does not mean that metal adatoms cannot exist on a graphene sheet. Indeed, McCreary and coworkers [74] have found indications of Au adatoms at a temperature of 18 K through temperature dependant Dirac point shifts, regardless of the very weak C↔Au interaction, yet Au clusters were observed by Atomic Force Microscopy (*AFM*) at room temperature. Aside, the E_{ads}/E_{coh} ratio has been previously proposed as a descriptor of the cluster growth, in 2D islands in the high ratio case, 3D nanoparticles in the low one [52,53].

Moreover, the difference between E_{coh} and E_{ads} is generally argued to be a descriptor of the metal aggregate coarsening [53]. In this sense, larger differences would indicate that TM atoms in an aggregate, cluster, or nanoparticle would require a significant high energy (temperature) to detach and adsorb on graphene. On the contrary, a small difference would indicate that such process would be easier. This has been used for instance to explain the Ostwald ripening process of AuPd nanoparticles deposited on a carbon support [75], suggesting that Pd atoms are, because of their easier detachability, the main vector in the

Ostwald ripening growth. Here we can argue as well that diffusion energy barriers would be no limiting step neither for Au nor Pd, being both below 0.05 eV, see Table 1, although the adsorption energy would play a role, *i.e.* Pd atoms would remain on the graphene surface at experimental temperatures, whereas Au adatoms could easily sublimate.

Present results however fail in describing the experimental better diffusivity of Co compared to Ni [44], although other theoretical studies show also larger E_{dif} values for Ni compared to Co [48,53,60], or, at most, similar diffusion barriers [52]. Indeed this difference can be explained in substrate terms, since STM experiments were carried out on a MLG graphene sheet, with a noticeable adhesion to the SiC substrate surface. Electronic or corrugation effects triggered by the substrate may alter the E_{dif} values by up to ~0.9, as theoretically found for 4*d* and 5*d* metals on graphene adsorbed on Ru(0001). Note that this is a substrate where graphene is physisorbed, and thus, features a faint corrugation and little electronic perturbation from the metal substrate surface. Stronger electronic effects are foreseen for chemisorbed graphene, on the contrary, and so, larger changes for diffusion energy barriers of atoms adsorbed on are to be expected. Thus, further research on Co and Ni diffusion on graphene explicitly adsorbed on SiC seems to be needed to gain a proper explanation of the experimental observations.

The previous trends seem to be unchanged by explicitly including vdW forces in the DF description, which anyway seems to have a substantial weight in E_{ads} for physisorbed d^5 or d^{10} adatoms. Indeed the energetic results for PBE-D2 calculations, gathered in Table 2, as well as *d* series trends, shown in Fig. 4, reveal practically no change in the overall picture described above. The addition of vdW only seems to increase E_{ads} values by ~0.35 eV in average, and so the trends closely follow the PBE ones, and same conclusions can be extracted from. One can compare present results with previous ones PBE-D2 and vdW-DF for Cu, Ag, [76] and also for Au [62]. The present E_{ads} estimates are ~0.35 eV smaller than

previous ones, which one could partly attribute to a smaller coverage of 0.02 ML in the previous study, and a slightly different computational set up. In any case, the trend of E_{ads} Cu ~ Au > Ag is in excellent agreement with the earlier study, yet slightly differs with the Cu > Au > Ag trend found at vdW-DF level, which in turns also deviates from PBE and LDA results.

Present results for Au and Cr are closer to the values obtained using the Tkatchenko-Scheffler (*Tk*) vdW correction [77], as obtained by Hardcastle *et al*. [63]. Indeed the differences are of solely 0.16 and 0.07 eV, respectively. However, the PBE-Tk results showed a stronger adsorption for Cr compared to Au, whereas the PBE-D2 forecasts both adsorptions to be similar in strength, see Table 2. Concerning the adsorption position, both previous works [62,63] highlight the similar E_{ads} values for H, B, and T positions, with preference for T site for Au and Cu, whereas H site is prognosticated for Ag and Cr, yet present results foresee B site occupancy. These structural aspects are discussed in depth in the next section.

3b. Structural Properties

Following the previous discussion, TM adatoms prefer, in general terms, to adsorb on H position, with the caveats of Ir, which prefers to adsorb on a h_1 site, yet still a hollow site. The H preference is mainly preferred for chemisorption situations, whereas a reduced coordination is found for physisorption situations; this is, for TMs with d^5 or d^{10} electronic configurations. Thus, for each hump along the *d* series one observes a coordination change from H→B→T. Here we note that Pd follows its d^{10} nature in this particular matter. Note that, for some metals such as Zn or Re, the energy differences between H, B, or T sites are minimal, almost negligible.

Putting aside previous works where site allocation was deliberately chosen to be H [48,49], present results mostly agree with the previous study by Habenicht *et al*. [59] for 4*d* and 5*d* metals, following the H→B→T trend, with the exception of weakly adsorbed metals

Ag, Re, where, as above stated, all these sites are essentially isoenergetic, and Ir, which in the previous study was found to occupy B sites, whereas here h_1 hollow site is found to be energetically most favoured. There is, however, disagreement with result from the work of Zólyomi *et al*. [58], who found for instance B sites for Mo, Pd, Pt, and Ag, and H for Mo and Au. On the other hand, a very good agreement with previous works is found for 3*d* metals, with very subtle deviations, such as placing Mn on H sites [50,53,55], or T site for Cr and Ag [50,52], although all these sites are really close in energy for such d^5 or d^{10} elements. More curious is the H prediction for Mo [52], Cr [54], and other d^5 elements [60], probably in the last case due to the neglect of spin polarization, which artificially produces overbonding of these elements on graphene.

All that said, the adsorption strength is connected to the site preference, and both intimately related to structural aspects. In particular, as observed in Fig. 5, a bump is observed for group VI and VII TMs, related mainly to their weaker adsorption, which sits the adatom further away from the graphene sheet. Here we must stress again that Tc prefers a smaller *h* because of the abnormally large adsorption energy, and that Re adjusts to this rule, but with a rather large height of more than 4 Å, due to the rather weak adsorption energy. This relation is also observed for groups XI and XII, with a clearly increased height due to the very weak E_{ads} values. Indeed, inset in Figure 5a shows how intimate is the relationship between *h* and E_{ads} values, and also provides a clear picture of how the TM height is similar for all the chemisorption situations.

The previous study at LDA level by Nakada and Ishii [60] predicted *h* values that are systematically shorter by 0.45 ± 0.53 Å, in line with the exceedingly large E_{ads} values. This is at variance with the *h* values obtained by a Ceperley-Alder [78] (*CA*) LDA xc functional *ab initio* molecular dynamics study by Wang *et al.* [54], who also found a systematic

Figure 5: Adsorption height, *h*, of 3*d*, 4*d*, and 5*d* TM adatoms on graphene as well as graphene corrugation, *c*, both in Å. Shown are the PBE (open circles and solid lines) and PBE-D2 (filled circles and dashed lines) DF results. Inset correlates *h* values with the adsorption energies, E_{ads}, in eV.

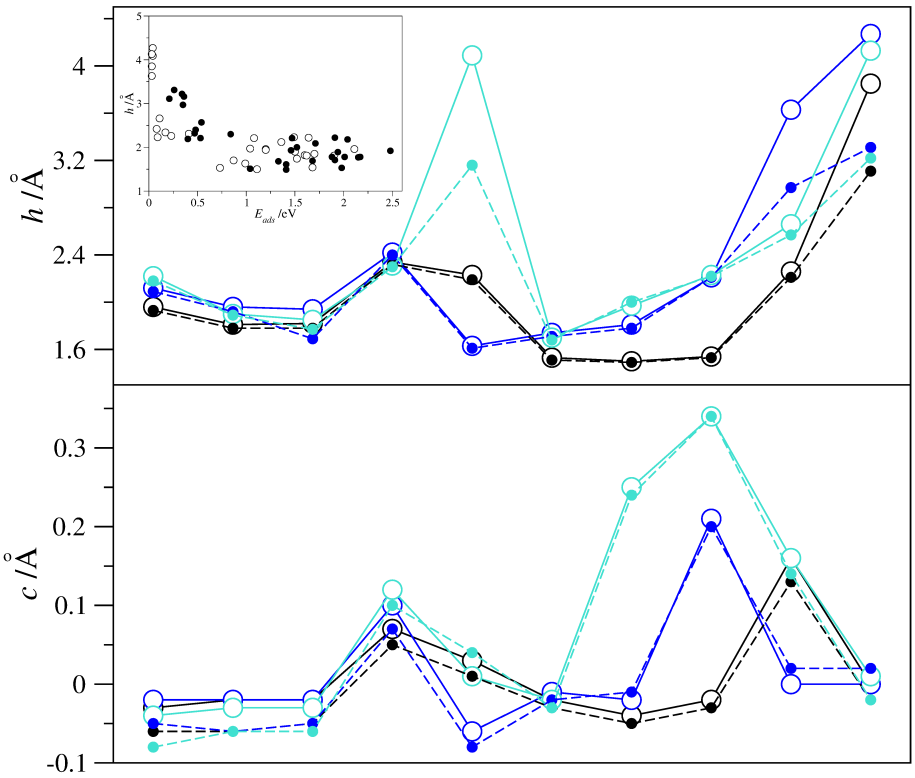

underestimation of 0.45 ± 0.53 Å. Underestimations were also found for PW91 [48] or PBE [49] calculations, but much more attenuated; of 0.10 ± 0.11 and 0.28 ± 0.34 Å, respectively. Similarly disperse values are found for other GGA works in the order of 0.1 ± 0.2 Å [52,55] being the work of Zólyomi *et al*. [58] the one with a somewhat larger discrepancy with the present values by roughly 0.25 ± 0.33 Å.

Corrugation values, as shown in Fig. 5, do also clearly reflect the adsorption site preference. Generally, adsorption on H sites produces a very small negative corrugation of 0.02-0.04 Å, where graphene embraces the TM adatom. Conversely, adsorption on T or B sites implies a pinning up of the C atoms involved in the adsorption by tenths of an Angstrom. This trend holds true except for the very weak adsorption strengths of d^5 or d^{10} TMs,

including Re, Ag, Zn, Cd, and Hg, all with E_{ads} below 0.04 eV. Aside from that it is worth to mention Pd and Pt cases —which chemisorb on B sites— with sensibly large corrugations of more than 0.2 Å, and also Ir, that, despite being accommodated on a h_1 hollow site, leads to a corrugation of 0.25 Å.

The addition of the D2 vdW correction has little effect on the structural aspects. Considering the site position, the addition of a description for dispersive forces has an effect only on physisorbed adatoms. In particular, Re prefers to adsorb on T when adding vdW, better adjusting to the H→B→T trend, and Hg prefers H position, similar to Zn. Aside from that, the vdW correction has a very little effect on *h* values, reducing it by 0.04 Å at most for chemisorbed adatoms, with the only caveat of Nb (0.25 Å) and Ta (0.08 Å), which can, nevertheless, be attributed to a forced change of the electronic configuration, see below. The decrease in height is more accentuated for physisorbed adatoms, where atoms get closer to the graphene sheet, by values above 0.9 Å in some cases (Cd, Re, Hg). As far corrugation is concerned, the addition of D2 yields a better embracement, with values increased by ~0.03 Å. Variations for pinned up graphene C atoms are of the same order.

Present results are in line with previous studies including a vdW description. Thus, PBE heights and vdW concomitant lowering are very similar to the values reported by Amft *et al*. at PBE-D2 and vdW-DF levels, with variations of ~0.1 Å at most [62]. Furthermore, a more significant *h* reduction is found for Ag compared to Au and Cu, as here also found. Curiously, PBE-Tk results by Hardcastle *et al*. [63] indicate that Au atoms are placed further away from the graphene layer, ~3.1 Å, whereas vdW-DF values with a similar adsorption energy, and also PBE-D2 indicate that Au would sit closer, at a distance of ~2.6 Å. On the other hand, PBE-Tk and present PBE-D2 *h* values for Cr are similar, ~2.1 and ~2.3 Å, respectively. Furthermore, the more distant situation of Au compared to Cr is also in agreement for both works.

Present results can be used to tackle the experimental evidence, although this is restricted to Ni and Co elements. Let us begin with Co adatoms; STM experiments on QFMLG assign the adsorption site to H, although the height from the graphene layers varies from 2.0 to 4.0 Å [32,47]. This is simply explained based on the fact that STM does not provide a direct measure of atomic heights but of the intensity *I*, which roughly stems out from the sum of orbitals sampled at a given tunnelling sample bias *V*. Nonetheless the height in the same experiment spans 2.0 to 2.4 Å depending on the V and I sampled, and previous theoretical simulations are textbook examples that electronic structure features are measured, and not the atomic structure *per se*, even if both are connected to some extent [79]. This particular aspect will be tackled in an oncoming study. Regardless of that, H position and moderate heights go side-to-side in present calculations.

The same H position is found for Ni, with an apparent height of 2.3-2.4 Å on a MLG [42,44]. Keep in mind that in this situation there is a non-negligible contact of the underlying SiC surface and the graphene sheet, which can modify the adsorptive properties of the latter, and actually this seems to be case, since same experiments on QFMLG yields two competitive situations for Ni adatom on graphene, H and T positions, with heights of 3.5 and 3.2 Å, respectively [41]. Something similar happens for Co, which is found to occupy T position on MLG at an apparent height of 3 Å, but again the two competitive situations H and T, with 3.1 and 2.2 Å apparent heights, respectively, on the QFMLG case.

Present results for Ni and Co on graphene show that H is, on both cases, the preferred adsorption site. The T site is located 0.61 and 0.31 eV higher in energy, respectively. One could argue that such difference is too large to have such sites populated in steady-state experimental conditions. In fact, experiments were carried out at 12 K, thus avoiding the Co or Ni adatom diffusion, and it could well happen that these adatoms could get trapped at these less stable positions, this being a common feature for adsorbed molecules at very low

temperatures [80]. However, within this reasoning B sites should be also populated, but they were never argued to be an adsorption site, although B and T sites could easily be confused given the close spatial proximity. A relatively easy experiment to corroborate so would be the mild warming of the system enabling diffusion of less stable B and T sites to more stable H ones, followed by a back cooling to 12 K and STM observation of a majority of H sites.

3c. Electronic and Magnetic Properties

Finally, electronic and magnetic properties are unfolded. The net charges obtained through a Bader analysis are plotted in Fig. 6. From it a clear trend can be withdrawn; all TMs —with the exception of Au— transfer electron density to the graphene layer. However, this charge transfer is more acute for early TMs, and more attenuated for late TMs. This behaviour can be easily explained based on Pauling electronegativities, which decay when going along a *d* series. This is applied in conjunction with the graphene electronegativity, or, viewed from another perspective, with the relative positions of graphene Fermi energy and the relative energies of TM *d* and *s* orbitals, which prompt such a charge transfer. In any case, TMs *n*-dope graphene, as experimentally observed for Ti, Fe, and Pt [36].

Moreover, present results highlight the special case of Au, whose very low electronegativity and high electron affinity prompts a graphene→Au charge transfer, and consequently, a *p*-doping of graphene. This is experimentally observed through a Dirac point shift into the unoccupied states region [37,39]. This *p*-doping is also predicted in other DF works, of the same ~0.1 e order [53,55]. These previous works show the same trends, although charge transfers are generally higher by 0.1-0.3 ± 0.1-0.3 e [48-50]. The work by Yazyez and Pasquarello show the trend, but at a higher coverage adatoms show a lower oxidation state by 0.23 ± 0.15 e [51]. Note in passing by that charged adatoms are thought to have an effect in dimer formation or larger cluster formation. According to this argument,

coulombic repulsion would go against dimer formation, and so, would support the existence of single adatoms, most at low temperatures. This would be more acute for earlier TMs, which feature the stronger oxidation state.

Figure 6: Oxidation state (Q), local magnetic moment (μ) and the change of the atomic magnetic moment ($\Delta\mu$) of 3*d*, 4*d*, and 5*d* TM adatoms om graphene. Units are as in Tables 1. Shown are the PBE (open circles and solid lines) and PBE-D2 (filled circles and dashed lines) DF results.

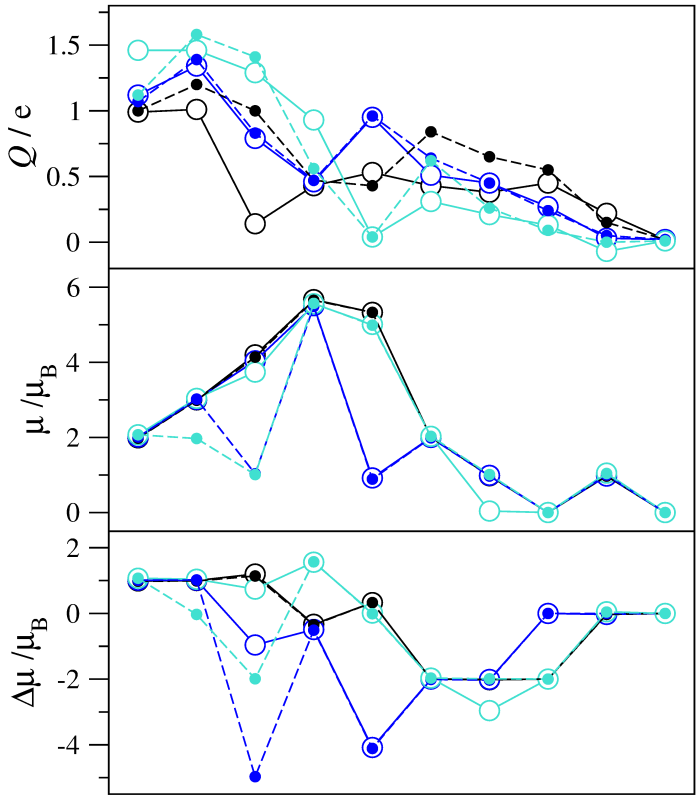

The vdW effect on the TM oxidation state is minimal, as observed in Fig. 6. Indeed, Q values differ by solely 0.06 e, this is, within the Bader analysis accuracy, and so, PBE and PBE-D2 values should be considered equal. This aligns with previous PBE-D2 and vdW-DF results on Cu, Ag, and Au [62]. Nevertheless, some caveats are necessary. The V adatom has, a priori, a very weak charge transfer as obtained at PBE, although addition of vdW forces description provides a value more in line with the overall trend. Aside from that, Tc is more

oxidized, in accordance to the enhanced adsorption strength, and, *vice versa*, Re is less oxidized, in line with the very weak interaction with graphene.

The charge transfer is intimately connected to the local magnetic moment variation, $\Delta\mu$, for early transition metals of groups III, IV, and, to a lesser extent, V and VI (see Tables 1 and 2, and Fig. 6). For these adatoms, the local magnetic moment, μ, increases due to a charge transfer of an *s* electron to the graphene bandstructure, which becomes coupled. Thus, the remaining TM *s* electron becomes uncoupled, and the local magnetic moment increases by ~1 μ_B. This goes along as well with the tabulated ionization states of the transition metal atoms. For later TMs this reasoning fails due to a competition between such ionization and a back donation process, as previously explained for 3*d* metals [50].

For d^5 TMs, the general outcome is a somewhat smaller charge transfer thus keeping the already stable d^5 configuration. Indeed this feature is preserved in late d^{10} TMs, including Pd. For the rest of the late TMs the μ values get generally reduced roughly by two. This can be easily explained from the TM→graphene charge transfer of the majority spin component, which becomes coupled in the graphene band structure, and a graphene→TM back donation in the minority spin component. This effect appears twice for Tc, thus leading to a much reduced local magnetic moment in comparison to that of the isolated atom. Another particular case is Nb due to the ground state s^1 d^4 configuration. Here, the TM→graphene charge transfer implies that the transferred electron density becomes coupled in the graphene band structure, with the concomitant reduction of the local magnetic moment. Finally, Ir seems to merge its electrons to the graphene electronic structure, yielding a diamagnetic ground state, although this statement requires further validation by a deeper analysis of the electronic structure.

In general terms, as seen in Fig. 6, μ increases along the *d* series up to reaching the d^5 elements. From this point on, there is an abrupt decrease of the magnitude of the magnetic

moment leading to small values or even to a non-magnetic ground state. In accordance with the calculated $\Delta\mu$ values, the abruptness is more remarkable in the case of Tc, and even more for Ir resulting in a diamagnetic ground state, at variance with other group IX (Co and Rh) elements. Here it is worth to point out that earlier experiments based on XMCD experiments [44] found that supported Fe and Co adatoms exhibit a paramagnetic ground state, whereas Ni adatoms are nonmagnetic, in excellent agreement with present results.

Note that addition of vdW description has very little effect on the magnetic properties, and indeed, for almost all the studied TMs, the calculated magnetic moment is essentially equal to that obtained with the standard PBE functional. There are some exceptions to this trend, Nb and Ta adatoms suffer an electronic configuration change induced by the small vdW forces. Indeed, Ta is no longer transferring an *s* electron to the graphene sheet, but suffering from the above-commented donation back-donation at different spin channels. This substantially reduces its μ to a value of *circa* 1 μ_B. In the case of Nb, this mechanism operates twice, as in the case of Tc, thus significantly quenching its magnetic moment. Aside, vdW seems to inhibit the *s* electron charge transfer of Hf, and, on the contrary, at the PBE-D2 level Ir is found to have a non-zero magnetic moment.

One has to keep in mind that vdW effect, rather than inhibiting/promoting a given electronic configuration, is changing the relative stability of the nearly degenerate multiple potential energy hypersurfaces corresponding to effective different electronic configurations for the adatom. In this repect, note that the electronic configuration of adsorbed Co can be controlled by a gate voltage [32,47], and indeed, calculations showed diverse configurations for Co on graphene, even at the same adsorption position, within an energy range of ~0.1 eV.[45] This is exactly the case also for Hf, Nb, and Ta, whose close different low spin configurations become, upon inclusion of *vdW* terms, slightly more stable than high spin ones by 0.1 eV at most, or, in the case of Ir, the high spin configuration is 0.06 eV more stable than

the non-magnetic one. These potential energy crossings should be the matter of a posterior study.

The overall trend described above was also already found in previous studies dealing with a fraction of the TM elements. Curiously, the coincidences seem to be highly connected to the coverage. Indeed, previous GGA studies at the same coverage yielded only small deviations of the order of 0.1 ± 0.1 μ_B [48,53,55]. However, the magnetism is somewhat quenched for slightly smaller or larger coverages of 0.02 [50] and 0.04 [52] ML, with reduction of local magnetic moments by 0.23 ± 0.39 and 0.54 ± 1.45 μ_B, respectively. This seems to suggest that local magnetic moment is optimal at the 0.03 ML coverage, although further assessment on this matter would be required to firmly confirm this point. In any case, for the rather large coverage of 0.17 ML, Zólyomi *et al*. clearly found a more acute reduction of the local magnetism by 1.50 ± 1.76 μ_B [58], a strong indication that a metal monolayer is being formed, with a delocalized band structure which favors pairing the *s* and *d* electrons.

4. Conclusions

Adsorption of transition metal atoms on graphene constitutes an attractive way of modifying their electronic and magnetic properties, with implications in spintronics, nanomagnetism, and data storage. Aside, the functionalization of graphene by TM adatoms may have repercussions in molecular storage, sensing, and, furthermore, these adatoms can be the building blocks or even the active sites of envisioned graphene-supported catalysts. Here we provide a thorough density functional theory study of the structural, energetic, diffusivity, magnetic, and electronic properties for the full sets of 3*d*, 4*d*, and 5*d* TM adatoms adsorbed on graphene, complementing the study with additional calculation including explicitly vdW

forces and thus determining their relative importance. This has been done by systematically sampling high and low symmetry adsorption sites and the diffusion among them.

Transition metal adatoms prefer to sit on H sites when chemisorbed, but the site preference shifts to B or T sites when physisorbed. The adsorption energy values follow a double hump trend, in which d^5 and d^{10} elements feature physisorption due to the isolated atom stability. The diffusion energy barriers go in consonance with the adsorption energies; the larger the adsorption energy, the larger the barrier to be overcome for diffusion. Despite E_{ads} values are increased by ~0.35 eV when adding vdW, the E_{dif} values remain overall constant.

The adatom height is governed by the adsorption strength, and therefore, physisorbed adatoms are located farther away from the graphene sheet (>2.3 Å) whereas chemisorbed atoms are located at *circa* 1.8 Å. These sit on H sites and prompt a graphene corrugation which embraces the TM adatom, whereas physisorbed TMs on B or T sites tend to pin up graphene C atom(s) by some tenths of an Å. Including dispersive forces merely approaches the physisorbed adatoms to the surface, in some cases by up to 1 Å.

TMs adatoms are found to *p*-dope the graphene layer, with the exception of Au, which *n*-dopes graphene. The doping degree decays when going along a given *d* series, due to the increase of Pauling electronegativity. The TM adatoms do also infer magnetism to the resulting adatom-graphene, specially the early ones, which indeed, see their local magnetic moments reinforced through electron donation/back-donation and coupling mechanisms. From d^5 elements on the magnetic moment abruptly decays, to a value of zero for late transition metals. Magnetism quenching mechanisms are highlighted, as well as the subtle interplay in between high and low spin states for selected transition metals, whose stability is in the order of the dispersive forces energy variations.

Finally, present results are compared to previous reports highlighting the effect of coverage, electron core, spin-orbit coupling, and the different employed levels of computation. Experimental observations such as adatom position, heights, clustering at different temperatures, Ostwald ripening growing vectors, the given *p*- or *n*-doping for specific adatoms, and even the electronic configuration at different sample gate voltages are rationalized by present calculations. Hence, present results provide a solid theoretical ground which provides the basis for interpreting and understanding already observed experimental features, but future findings as well.

Acknowledgements

This work was supported by Spanish *Ministerio* grant CTQ2012-30751 and *Generalitat de Catalunya* grants (2014SGR97 and XRQTC). F.V. thanks the Spanish *Ministerio de Economía y Competitividad* for the *Ramón y Cajal* (RyC) postdoctoral grant (RYC-2012-10129).

References

[1] Novoselov KS, Geim AK, Morozov SV, Jiang D, Zhang Y, Dubonos SV, et al. Electric field effect in atomically thin carbon films. Science 2004;306:666-9.

[2] Castro Neto AH, Guinea F, Peres NMR, Novoselov KS, Geim AK. Covalent functionalization of strained graphene. Rev Mod Phys 2009;81:109-62.

[3] Geim AK. Graphene: Status and prospects. Science 2009;324:1530-4.

[4] Sofo JO, Chaudhari AS, Barber GD. First-principles study of half metallicity in semi hydrogenated BC_3, BC_5, BC_7, and B-doped graphone sheets. Phys Rev B 2007;75:153401.

[5] Cheng J-H, Zou K, Okino F, Gutierrez HR, Gupta A, Shen N, et al. Tuning the electronic transport properties of graphene through functionalisation with fluorine. Phys Rev B 2010;81:205435.

[6] Loh KP, Bao Q, Eda G, Chhowalla M. Graphene oxide as a chemically tunable platform for optical applications. Nat Chem 2010;2:1015-24.

[7] Kozlov SM, Viñes F, Görling A. Bandgap engineering of graphene by physisorbed adsorbates. Adv Mater 2011;23:2638-43.

[8] Kozlov SM, Viñes F, Görling A. On the interaction of polycyclic aromatic compounds with graphene. Carbon 2012;50:2482-92.

[9] Schedin F, Geim AK, Morozov SV, Hill EW, Blake P, Katsnelson MI, et al. Detection of individual molecules adsorbed on graphene. Nat Mater 2007;6:652-5.

[10] N'Diaye AT, Bleikamp S, Feibelman PJ, Michely T. Two-dimensional Ir cluster lattice on a graphene moiré on Ir(111). Phys Rev Lett 2006;97:215501.

[11] Karimi S, Tavasoli A, Mortazavi Y, Karimi A. Cobalt supported on graphene – A promising novel Fischer–Tropsch synthesis catalyst. Appl Catal A: General 2015:499;188-96.

[12] Lee S, Fan C, Wu T, Anderson SL. CO Oxidation on Au_n/TiO_2 catalysis by size selected cluster deposition J Am Chem Soc 2004;126:5682-3.

[13] Vajda S, Pellin MJ, Greeley JP, Marshall CL, Curtiss LA, Ballentine GA, et al. Subnanometre platinum clusters as highly active and selective catalysts for the oxidative dehydrogenation of propane. Nat Mater 2009;8: 213-6.

[14] Kong J, Chapline MG, Dai H. Functionalized carbon nanotubes ofr molecular Hydrogen sensors. Adv Mater 2001;13:1384-6.

[15] Collins PG, Bradley K, Ishigami M, Zettl A. Extreme oxygen sensitivity of electronic properties of carbon nanotubes. Science 2000;287:1801-4.

[16] Mota R, Fagan SB, Fazzio A. First principles study of titanium-coated carbon nanotubes as sensors for carbon monoxide molecules. Surf Sci 2007;601:4102-4.

[17] Yildirim T, Ciraci S. Titanium-decorated nanotubes as a potential high capacity Hydrogen storage medium. Phys Rev Lett 2005;94:175501.

[18] Sun Q, Wang Q, Jena P, Kawazoe Y. Clustering of Ti on a C_{60} surface and its effect on hydrogen storage. J Am Chem Soc 2005;127:14582-3.

[19] Chandrakumar KRS, Ghosh SK. Alkali-metal-induced enhancement of hydrogen adsorption in C_{60} fullerene: An ab initio study. Nano Lett 2008;8:13-9.

[20] Hupalo M, Liu XJ, Wang CZ, Lu WC, Yao YX, Ho KM, et al. Metal nanostructure formation on graphene: Weak versus strong bonding. Adv Mater 2011;23:2082-7.

[21] Planeix JM, Coustel N, Coq B, Brotons V, Kumbhar PS, Dutartre R, et al. Application of carbon nanotubes as supports in heterogeneous catalysis. J Am Chem Soc 1994;116:7935-6.

[22] Lordi V, Yao N, Wei J. Method for supporting platinum on single-walled carbon nanotubes for a selective hydrogenation catalyst. Chem Mater 2001;13:733-7.

[23] Li Y, Zhou Z, Yu G, Chen W, Chen Z. CO catalytic oxidation on iron-embedded graphene: Computational quest for low-cost nanocatalysts. J Phys Chem C 2010;114:6250-4.

[24] Ajayan PM, Lijima S. Capillarity-induced filling of carbon nanotubes. Nature 1993;361:333-4.

[25] Javey A, Guo J, Farmer DB, Wang Q, Wang D, Gordon RG, et al. Carbon nanotube field-effect transistors with integrated ohmic contacts and high-κ gate dielectrics. Nano Lett 2004;4:447-50.

[26] Son YW, Cohen ML, Louie SG. Half-metallic graphene nanoribbons. Nature 2006;444:374-7.

[27] Karpan VM, Giovannetti G, Khomyakov PA, Talanana M, Starikov AA, Zwierzycki M, et al. Graphite and graphene as perfect spin filters. Phys Rev Let 2007;99:176602.

[28] Tombros N, Jozsa C, Popinciuc M, Jonkman H.T, van Wees BJ. Electronic spin transport and spin precession in single graphene layers at room temperature. Nature 2007;448:571-4.

[29] Geim AK, Novoselov KS. The rise of graphene. Nat Mater 2007;6:183-91.

[30] Xiao RJ, Fritsch D, Kuz'min MD, Koepernik K, Eshrig H, Richter M, et al. Co dimers on hexagonal carbon rings proposed as subnanometer magnetic storage bits. Phys Rev Lett 2009;103:187201.

[31] Berashevich J, Chakraborty T. Tunable band gap and magnetic ordering by adsorption of molecules on graphene. Phys Rev B 2009;80:033404.

[32] Brar VW, Decker R, Solowan H-M, Wang Y, Maserati L, Chan KT, et al. Gate-controlled ionization and screening of cobalt adatoms on a graphene surface. Nat Phys 2011;7:43-7.

[33] Zanella I, Fagan SB, Mota R, Fazzio A. Electronic and magnetic properties of Ti and Fe on graphene. J Phys Chem C 2008;112:9163-7.

[34] Lima MP, da Silva AJR, Fazzio A. Adatoms in graphene as a source of current polarization: Role of the local magnetic moment. Phys Rev B 2011;84:245411.

[35] Liu X, Wang CZ, Yao YX, Lu WC, Hupalo M, Tringides MC, et al. Bonding and charge transfer by metal adatom adsorption on graphene. Phys Rev B 2011;83:235411.

[36] Pi K, McCreary KM, Bao W, Han W, Chiang YF, Li Y, et al. Electronic doping and scattering by transition metals on graphene. Phys Rev B 2009;80:075406.

[37] McCreary KM, Pi K, Swartz AG, Han W, Bao W, et al. Effect of cluster formation on graphene mobility. Phys Rev B 2010;81:115453.

[38] Wang B, Yoon B, König M, Fukamori Y, Esch F, Heiz U, et al. Size-selected monodisperse nanoclusters on supported graphene: Bonding, isomerism, and mobility. Nano Lett 2012;12:5907-12.

[39] Gierz I, Riedl C, Starke U, Ast CR, Kern K. Atomic hole doping of graphene. Nano Lett 2008;8:4603-7.

[40] Chen J-H, Jang C, Adam S, Fuhrer M.S, Williams ED, Ishigami M. Charged impurity scattering in graphene. Nat Phys 2008;4:377-81.

[41] Eelbo T, Waśniowska M, Gyamfi M, Forti S, Starke U, Wiesendanger R. Influence of the degree of decoupling of graphene on the properties of transition metal adatoms. Phys Rev B 2013;87:205443.

[42] Gyamfi M, Eelbo T, Waśniowska M, Wehling TO, Forti S, Starke U, et al. Orbital selective coupling between Ni adatoms and graphene Dirac electrons. Phys Rev B 2012;85:161406.

[43] Uchoa B, Yang L, Tsai S-W, Peres NMR, Castro Neto AH. Orbital symmetry fingerprints for magnetic adatoms in graphene. New J Phys 2014;16:013045.

[44] Eelbo T, Waśniowska M, Thakur P, Gyamfi M, Sachs B, Wehling TO, et al. Adatoms and clusters of 3d transition metals on graphene: electronic and magnetic configurations. Phys Rev Lett 2013;110:136804.

[45] Virgus Y, Purwanto W. Krakauer H, Zhang S. Stability, energetics, and magnetic states of Cobalt adatoms on graphene. Phys Rev Lett 2014;113:175502.

[46] Wehling TO, Lichtenstein AI, Katsnelson MI. Transition-metal adatoms on graphene: Influence of local Coulomb interactions on chemical bonding and magnetic moments. Phys Rev B 2011;84:235110.

[47] Donati F, Dubout Q, Autès G, Patthey F, Calleja F, Gambardella P, et al. Magnetic moment and anisotropy of individual Co atoms on graphene. Phys Rev Lett 2013;111:236801.

[48] Valencia H, Gil A, Frapper G. Trends in the adsorption of 3d transition metal atoms onto graphene and nanotube Surfaces: A DFT study and molecular orbital analysis. J Phys Chem C 2010;114:14141–53.

[49] Sargolzaei M, Gudarzi F. Magnetic properties of single 3d transition metals adsorbed on graphene and benzene: A density functional theory study. J Appl Phys 2011;110:064303.

[50] Zhang T, Zhu L, Yuan S, Wang J. Structural and magnetic properties of 3d transition-metal-atom adsorption on perfect and defective graphene: A density functional theory study. ChemPhysChem 2013;14:3483-8.

[51] Yazyev OV, Pasquarello A. Metal adatoms on graphene and hexagonal boron nitride: Towards rational design of self-assembly templates. Phys Rev B 2010;82:045407.

[52] Hu L, Hu X, Wu X, Du C, Dai Y, Deng J. Density functional calculation of transition metal adatom adsorption on graphene. Physica B 2010;405:3337-41.

[53] Liu X, Wang CZ, Hupalo M, Lu WC, Tringides MC, Yao YX, et al. Metals on graphene: Correlation between adatom adsorption behavior and growth morphology. Phys Chem Chem Phys 2012;14:9166-75.

[54] Wang Z, Niu X, Su Q, Deng H, Li Z, Hu W, et al. Transition metal adsorption promotes patterning and doping of graphene by electron irradiation. J Phys Chem C 2013;117:17644-9

[55] Ding J, Qiao Z, Feng W, Yao Y, Niu Q. Magnetic and electronic properties of metal-atom adsorbed graphene. Phys Rev B 2011;84:195444.

[56] Ishii A, Yamamoto M, Asano H, Fujiwara K. DFT calculation for adatom adsorption on graphene sheet as a prototype of carbon nanotube functionalization. J Phys: Conf Ser 2008;100:052087.

[57] Zhang H, Lazo, C, Blügel S, Heinze S, Mokrousov Y. Electrically tunable quantum anomalous hall effect in graphene decorated by 5d transition-metal adatoms. Phys Rev Lett 2012;108:056802.

[58] Zólyomi V, Rusznyák Á, Kürti J, Lambert CJ. First principles study of the binding of 4d and 5d transition metals to graphene. J Phys Chem C 2010;114:18548-52.

[59] Habenicht BF, Teng D, Semidey-Flecha L, Sholl DS, Xu Y. Top Catal 2014;57:69-79.

[60] Nakada K, Ishii A. Effect of mono-vacancy on transport properties of zigzag carbon- and boron-nitride-nanotube heterostructures. Sol State Commun 2011;151:13-16.

[61] Virgus Y, Purwanto W, Krakauer H, Zhang S. Ab initio many-body study of cobalt adatoms adsorbed on graphene. Phys Rev B 2012;86:241406.

[62] Amft M, Lèbegue S, Eriksson O, Skorodumova NV. Small gold clusters on graphene, their mobility and clustering: a DFT study. J Phys: Condens Matter 2011;23:205301.

[63] Hardcastle TP, Seabourne CR, Zan R, Brydson RM, Bangert U, Ramasse QM, et al. Mobile metal adatoms on single layer, bilayer, and trilayer graphene: An ab initio DFT study with van der Waals corrections correlated with electron microscopy data. Phys Rev B 2013;87:195430.

[64] Kresse G, Furthmüller J. Efficient iterative schemes for ab initio total-energy calculations using a plane-wave basis set. Phys Rev B 1996;54:11169-86.

[65] Blöchl PE. Projector augmented-wave method. Phys Rev B 1994;50:17953-79.

[66] Perdew JP, Burke K, Ernzerhof M. Generalized gradient approximation made simple. Phys Rev Lett 1996;77:3865-8.

[67] Janthon P, Viñes F, Kozlov SM, Limtrakul J, Illas, F. Theoretical assessment of graphene-metal contacts. J Chem Phys 2013;183:244701.

[68] Janthon P, Kozlov SM, Viñes F, Limtrakul J, Illas F. Establishing the accuracy of broadly used density functionals in describing bulk properties of transition metals. J Chem Theory Comput 2013;9;1631-40.

[69] Janthon P, Luo SJ, Kozlov SM, Viñes F, Limtrakul J, Truhlar DG, et al. Bulk Properties of transition metals: A challenge for the design of universal density functionals. J Chem Theory Comput 2014;10:3832-9.

[70] Monkhorst HJ, Pack JD. Special points for Brillouin-zone integrations. Phys Rev B 1976;13:5188-92.

[71] Bader RF. Atoms in Molecules: A Quantum Theory, Oxford Science, Oxford, U.K. 1990.

[72] Grimme S. Semiempirical GGA-type density functional constructed with a long-range dispersion correction. J. Comp Chem 2006;27:1787-99.

[73] Viñes F, Borodin A, Hofft O, Kempter V, Illas, F. The interaction of CO_2 with sodium-promoted W(011). Phys Chem Chem Phys 2005;7:3866-73.

[74] McCreary KM, Pi K, Swartz AG, Han W, Bao W, Lau CN, et al. Effect of cluster formation on graphene mobility. Phys Rev B 2010;81:115453.

[75] Nelayah J, Nguyen NT, Alloyeau D, Wang GY, Ricolleau C. Long-range chemical orders in Au–Pd nanoparticles revealed by aberration-corrected electron microscopy. Nanoscale 2014;6:10423-30.

[76] Dion M, Rydberg H, Schröder E, Langreth D, Lundqvist B. Van der Waals density functional for general geometries. Phys Rev Lett 2004;92:246401.

[77] Tkatchenko A, Scheffler M. Accurate Molecular Van der Waals interactions from ground-state electron density and free-atom reference data. Phys Rev Lett 2009;102:073005.

[78] Ceperley DM, Alder BJ. Ground state of the electron gas by a stochastic method. Phys Rev Lett 1980;45:566-9.

[79] Nilius N, Kozlov SM, Jerratsch JF, Baron M, Shao X, Viñes F, et al. Formation of one-dimensional electronic states along the step edges of CeO_2(111). ACS Nano 2012;6:1126-33.

[80] Happel M, Luckas N, Viñes F, Sobota M, Laurin M, Görling A, et al. SO_2 Adsorption on Pt(111) and oxygen pre-covered Pt(111): A combined infrared reflection absorption spectroscopy and density functional study. J Phys Chem C 2011;115:479-91.